Evidence for Conformational Changes upon Copper Binding to Cupriavidus metallidurans CzcE

ARTICLE *in* BIOCHEMISTRY · MARCH 2010

Impact Factor: 3.02 · DOI: 10.1021/bi100001z · Source: PubMed

7 AUTHORS, INCLUDING:

Isabelle Petit-Haertlein
Institut de Biologie Structurale (IBS)
29 PUBLICATIONS **453** CITATIONS

SEE PROFILE

Eric Girard
Atomic Energy and Alternative Energies Com…
61 PUBLICATIONS **651** CITATIONS

SEE PROFILE

BIOCHEMISTRY
including biophysical chemistry & molecular biology
Article

Biochemistry **2010,** *49,* 1913–1922 1913
DOI: 10.1021/bi100001z

Evidence for Conformational Changes upon Copper Binding to *Cupriavidus metallidurans* CzcE‡

Isabelle Petit-Haertlein,§,# Eric Girard,§,# Géraldine Sarret,∥ Jean-Louis Hazemann,⊥ Patrick Gourhant,@ Richard Kahn,§ and Jacques Covès*,§

§*Institut de Biologie Structurale-Jean-Pierre Ebel, UMR 5075 CNRS-CEA-UJF, 41, rue Jules Horowitz, 38027 Grenoble Cedex, France,* ∥*Equipe de Géochimie de l'Environnement, LGIT-UMR 5559 CNRS-UJF, BP 53, 38041 Grenoble Cedex 9, France,* ⊥*Institut Néel, 25 avenue des Martyrs, BP 166, 38042 Grenoble Cedex 9, France, and* @*Synchrotron SOLEIL, Proxima-1, L'Orme des Merisiers, Saint-Aubin, BP48, 91192 Gif-sur-Yvette Cedex, France.* #*These authors contributed equally to this work.*

Received January 1, 2010; Revised Manuscript Received January 28, 2010

ABSTRACT: CzcE is a periplasmic protein from *Cupriavidus metallidurans* CH34 that can bind four copper atoms per dimer. We have crystallized the apo form of the protein and determined its structure at 1.85 Å resolution. Three Cu atoms were localized by soaking apo-CzcE crystals into a $CuCl_2$ solution. We identified His24 as a Cu(II) ligand in each protomer and Asp100 as a key residue for Cu binding at the interface of the dimer. The role of these amino acids was confirmed by site-directed mutagenesis and UV−visible spectroscopy. The fourth Cu atom was not located. The oxidized form of CzcE contains four Cu(II) atoms, while the reduced form contains four Cu(I) atoms. Average coordination spheres of four N or O atoms for Cu(II) and of one N or O atom and two S atoms for Cu(I) were determined by X-ray absorption spectroscopy. As there is no evidence for preformed metal-binding sites in apo-CzcE, we suggest that different conformational changes occurred upon Cu(II) or Cu(I) binding. These changes were further demonstrated by digestion experiments that gave different proteolysis patterns depending not only on the presence of the metal but also on its speciation. The ability of CzcE to bind copper and to adapt its conformation to different copper oxidation states could be related to a role in copper sensing for this protein.

Cupriavidus metallidurans CH34 is exceptionally well equipped to resist high concentrations of many heavy metals (*1*−*6*). For this reason, applications of this strain to microbial ecology and environmental biotechnology were developed (*7*, *8*). Moreover, because its genome has been sequenced, it can be considered as the archetypical strain for understanding metal homeostasis or metal resistance phenotypes (*5*, *9*). For instance, the *czc* determinant confers to *C. metallidurans* CH34 the ability to modulate its internal concentrations of cobalt, zinc, and cadmium (*10*−*13*). It consists of a cluster of nine genes, *czcNICBADRSE*, enrolled in the expression of the efflux pump CzcCBA through sophisticated control circuits that are not fully understood (*12*). Surprisingly, the product of the *czcE* gene is a small periplasmic metal-binding protein that has been recently reported to be specific for copper ions (*14*). CzcE could be a copper sensor linking the copper and the cobalt, zinc, and cadmium resistance in *C. metallidurans* CH34. Interestingly, *czcE* would have appeared in the *czc* determinant after duplication of the *copH* gene (*9*), itself part of the copper resistance system of *C. metallidurans* CH34 (*1*, *3*−*5*). CzcE and CopH are thus strain-specific paralogs but have some important differences. While these two proteins are 53% similar, including 38% identical in their mature forms, CzcE is shorter than CopH because it lacks ∼20 amino acids suggested to be unstructured in CopH (*16*). CopH is a dimeric protein able to specifically bind two copper ions per dimer with high affinity (*16*). Its two histidine residues, His24 and His26, are both involved in copper binding. They contribute to the nitrogen environment of the equatorial plane for the two Cu(II) type 2 centers. In contrast, CzcE contains only one His in a position that can be aligned with His26 in CopH. With regard to the other amino acids frequently involved in copper binding, a major difference between these two proteins is that CzcE possesses five methionine residues and CopH none. Furthermore, none of these proteins contains any cysteine residues.

CzcE was previously shown to bind 4 equiv of copper per dimer (*14*). We have suggested that CzcE was able to accept four Cu(II) ions in four spectroscopically indistinguishable sites characteristic of type 2 copper with typical Cu(II) d−d transitions. Reduction of the four Cu(II) ions by addition of ascorbate led to the fully reduced form containing four Cu(I) atoms. After reoxidation in air, an air-stable semireduced form of the protein containing two Cu(I) and two Cu(II) ions was obtained. The spectroscopic characteristics of the semireduced form were slightly but significantly different from those of the fully oxidized form as judged from both the bathochromic shift of the electronic transition and the values of EPR[1] parameters. Both the stabilization of two Cu(I) ions in the semireduced form and the modification of the coordination of Cu(II) deduced from the new spectroscopic parameters can be interpreted by conformational changes in the polypeptide chain providing new ligands and/or different geometries.

‡Coordinates and structure factors have been deposited in the Protein Data Bank as entries 2wto for apo-CzcE and 2wtp for Cu-bound CzcE.

*To whom correspondence should be addressed. Telephone: 33-(0)4-38-78-24-03. Fax: 33-(0)4-38-78-54-94. E-mail: jacques.coves@ibs.fr.

[1]Abbreviations: EXAFS, extended X-ray absorption fine spectroscopy; SAD, single-wavelength anomalous diffraction; TLS, translation libration screw; XANES, X-ray absorption near-edge structure; XAS, X-ray absorption spectroscopy; EPR, electron paramagnetic resonance.

Published on Web 01/29/2010

As yet, it has not been possible to obtain crystals of the copper-bound form of CzcE. In this paper, we describe the X-ray structure of apo-CzcE and of a metalled form of CzcE obtained via addition of Cu(II) in the crystalline state. This approach was coupled to X-ray absorption experiments on either the fully oxidized or the fully reduced form of CzcE and to protease susceptibility as a function of the copper speciation to highlight conformational changes linked to copper binding.

MATERIALS AND METHODS

Expression and Purification of CzcE and Its Derivatives. CzcE was overproduced as a periplasmic protein in its mature form starting with Leu24 (spanning residues 24−131) in *Escherichia coli* BL21(DE3) as previously described (*14*, *16*). Primers used for directed mutagenesis were designed to replace His24 with alanine (5′-CAGGCGATGGCGAAGCGTGCCGCGACCTTG-3′ and 5′-CAAGGTCGCGGCACGCTTCGCCATCGCCTG-3′) or Asp100 with asparagine (5′-GGCGTGCGCGTCTATATTAATAGAAGCGACCTCT-3′ and 5′-AGAGGTCGCTTCTATTAATATAGACGCGCACGCC-3′) to produce H24A- or D100N-CzcE, respectively. The mismatch regions corresponding to the replacement of the CAT codon (His) with GCC (Ala) and of the GAT codon (Asp) with AAT (Asn) are underlined. The overexpression plasmid pET-CzcE was used for each single mutation. The QuikChange site-directed mutagenesis kit from Stratagene was used as specified by the manufacturer. Mutations were confirmed by DNA sequencing, and the new constructs were transformed into *E. coli* BL21(DE3) for overexpression of the corresponding protein under the conditions used for native CzcE (*14*, *16*). The selenomethionine derivative of CzcE was expressed the same way in purposely defined growth conditions (*17*). The experimental masses of the CzcE mutants and Se-CzcE were checked by mass spectrometry to ascertain the mutations and the correct substitution of the five methionine residues of CzcE with selenomethionine, respectively. Native CzcE, H24A-CzcE, D100N-CzcE, and Se-CzcE were purified by a combination of ammonium sulfate precipitation and gel filtration as previously described (*16*). Protein concentrations were determined by using an extinction coefficient of 12071 M^{-1} cm^{-1} deduced from the total amino acid composition as described previously (*18*).

Crystallization, Soaking, and Data Collection. Crystals of native CzcE and Se-CzcE were obtained under conditions refined from those defined previously (*16*). Briefly, 7 μL of protein at 13.2 mg/mL was mixed with 3 μL of a reservoir solution composed of 32−34% PEG4000, 0.1 M Tris-HCl (pH 8.5), 200 mM $MgCl_2$, and 10% glycerol. The drop was equilibrated against 800 μL of reservoir solution. Crystals appeared in approximately 2−3 weeks using the sitting-drop vapor-diffusion method at 293 K. For soakings in the presence of copper, a 10 mM solution of $CuCl_2$ in water was directly added to a drop containing crystals and incubated for 36 h with two consecutive additions of 1 μL at 2 h intervals followed by an overnight incubation and the consecutive additions of 1 and 2 μL followed by a new overnight incubation. Before data collection, crystals were harvested in a cryoloop and frozen in liquid nitrogen.

The X-ray diffraction data set for crystals of Se-CzcE was collected to a resolution of 1.60 Å (Table 1) at beamline ID29 (European Synchrotron Radiation Facility, Grenoble, France). On the basis of fluorescence measurement, the wavelength was set at 0.97961 Å, corresponding to the maximum value of f'' in the Se-K absorption for a SAD experiment. Both native CzcE crystals and Cu(II)-soaked crystals were used to collect diffraction data at beamline Proxima-1 (Soleil synchrotron, Saclay, France). The apo-CzcE crystal diffracted to 1.85 Å resolution. Two data sets were collected with the copper-soaked CzcE crystals. One data set was collected at the K absorption edge of Cu and was used to localize the Cu atoms by using their anomalous signal. The second data set was collected at a wavelength of 0.98 Å and was used to refine the structure of Cu-bound CzcE to a resolution of 1.50 Å. Diffraction data were integrated with *XDS* (*19*) and scaled and merged with *SCALA* and *TRUNCATE* from the CCP4 suite (*20*). All crystals belonged to space group *C*2. Integration statistics are listed in Table 1. Assuming the presence of two molecules of CzcE per asymmetric unit, the Matthews coefficient (*21*) was 2.16 $Å^2$/Da, with an estimated solvent content of 35%.

Structure Determination and Refinement. Se-SAD phasing was performed using *AutoSHARP* (*22*). The Se substructure was determined with *SHELXD* (*23*). Eight selenium atom were localized, over the 10 expected from the selenomethionines from two CzcE molecules in the asymmetric unit. The Se substructure was refined, and initial phases were calculated with *SHARP* (*24*). The initial SAD phases were improved by density modification using *SOLOMON* (*25*) and *DM* (*26*). Automatic building, performed with *Arp*/*Warp* (*27*), permitted docking of 175 residues over the 216 anticipated for two CzcE molecules per asymmetric unit. Refinement of the Se-CzcE structure revealed evidence of radiation damage. Thus, in spite of the higher resolution of the Se-Cze data, final refinement was performed on the data recorded with crystals of apo-CzcE. Using the automatically built model as a starting point, structures of both the apo form and the Cu-bound form of CzcE were refined with *phenix.refine* (*28*). Structure inspections and manual binding were performed using *Coot* (*29*). The same 5% set of reflections were excluded from automatic building and were withheld during the two refinement processes to monitor the R_{free} value (*30*). Water molecules were automatically generated by the procedure *phenix.refine* looking for peaks greater than 1σ in the $2F_o - F_c$ electron density map that were fulfilling the default geometric criteria. The generated water molecules were manually checked using *Coot*. Translation libration screw (TLS) refinement was performed. TLS, by better accounting for correlated movements within the molecules, led to less noisy $F_o - F_c$ difference Fourier maps and to better-controlled differences between R_{free} and R_{work} factors versus classical TLS-free refinements. TLS groups were determined using the TLSMD server (*31*). Six and five TLS groups per monomer were used for the apo and Cu-bound structures, respectively. Atomic displacement parameters for Cu, Mg, and chloride atoms were refined anisotropically. The final statistics for both structures are given in Table 1.

Spectroscopic Methods. UV−visible spectroscopy was used as previously described (*14*) to follow the titration of native CzcE or its mutants with $CuCl_2$. The proteins were routinely used at a concentration of 0.25 mM for these experiments. For XAS experiments, samples of CzcE at 1.35 mM were prepared in a final volume of 120 μL and contained 15% glycerol. Cu(II)-bound CzcE was prepared by addition of 5.4 mM $CuCl_2$. Fully reduced CzcE was obtained by addition of 10 molar equiv of sodium ascorbate. The semireduced form was produced by reoxidation in air of CzcE previously reduced by addition of 2 molar equiv of sodium ascorbate. The correct metalation of the protein and the different speciation states were checked by visible

Table 1: Data Collection, Phasing, and Structural Refinement Statistics

	Se form	apo form	Cu-bound form
Data Collection Statistics			
cell parameters	a = 105.930 Å b = 29.510 Å c = 71.250 Å β = 113.815°	a = 105.427 Å b = 29.610 Å c = 70.961 Å β = 113.756°	a = 105.000 Å b = 29.530 Å c = 71.170 Å β = 113.412°
resolution (Å) (high-resolution shell)	48.45−1.60 (1.68−1.60)	48.22−1.85 (1.94−1.85)	19.14−1.50 (1.58−1.50)
R_{merge}[a] (%) (high-resolution shell)	6.5 (30.2)	4.1 (13.4)	4.2 (24.4)
$I/\sigma(I)$[b] (high-resolution shell)	11.5 (3.6)	22.8 (9.7)	17.6 (5.5)
completeness (%) (high-resolution shell)	99.1 (94.4)	99.6 (97.3)	99.4 (97.9)
multiplicity (high-resolution shell)	3.6 (3.5)	3.7 (3.6)	3.9 (3.9)
Phasing Statistics			
phasing power	1.744		
FOM after *Sharp*	0.347		
FOM after *DM*	0.842		
Refinement Statistics			
data range (Å)		48.22−1.85	19.14−1.50
no. of reflections		17541	32477
R_{work}[c]		0.1635	0.1599
R_{free}[c]		0.1921	0.1885
R_{total}[c]		0.1649	0.1613
root-mean-square deviation from ideal positions[d]			
bond lengths (Å)		0.012	0.026
bond angles (deg)		1.325	2.448
no. of protein atoms		1428	1421
no. of Cu atoms		−	3
no. of Mg atoms		1	1
no. of Cl atoms		10	10
no. of solvent atoms		233	200
$\langle B \rangle$[e] for protein atoms (Å^2)		15.9	18.9
$\langle B \rangle$[e] for solvent atoms (Å^2)		27.8	33.9
$\langle B \rangle$[e] for Cl atoms (Å^2)		25.8	22.6
$\langle B \rangle$[e] for Mg atoms (Å^2)		22.3	15.2
occupancy of Mg		0.80	0.70
$\langle B \rangle$[e] (Å^2)/occupancy for Cu atoms			
Cu1 (Asp100)		−	13.2/0.65
Cu2 (His24 A)		−	37.7/0.40
Cu3 (His24 B)		−	21.7/0.20

[a] $R_{merge} = \sum_h \sum_i |I(h) - I_i(h)| / \sum_h \sum |I_i(h)|$, where $I_i(h)$ is the ith measurement of reflection h and $I(h)$ is the mean measurement of reflection h. [b] $I/\sigma(I)$ is the signal-to-noise ratio for merged intensities. [c] $R = \sum_h |F_o - F_c| / \sum_h |F_o|$, where F_o and F_c are the observed and calculated structure factor amplitudes of reflection h, respectively. R_{free} is the R for the test reflection data set for cross validation (ref). R_{work} is the R for the working reflection data set, and R_{total} is the R for all of the data. [d] Calculated with *phenix.refine*. [e] The B values shown refer to the isotropic equivalent of the anisotropic thermal parameters used during refinement.

spectrophotometry. For XAS experiments, 100 μL of each sample was transferred right after preparation to a PEEK homemade five-cell sample holder with a Kapton window and flash-frozen in liquid nitrogen.

X-ray absorption measurements were taken at the European Synchrotron Radiation Facility which was operating with a ring current of 150−200 mA. Spectra were collected on the BM30B (FAME) beamline (*32*) using a Si(220) double-crystal monochromator with dynamic sagital focusing. The photon flux was on the order of 10^{12} photons/s, and the spot size was 300 μm horizontal × 50 μm vertical. The sample holder was loaded in a helium cryostat with the temperature set to 10 K during data collection. All spectra were recorded in fluorescence mode by measuring the Cu-Kα fluorescence with a 30-element solid-state Ge detector (Canberra). For each sample, 10−15 scans of 40 min each were averaged. Data from each detector channel were inspected for glitches or drop-outs before inclusion in the final average.

Energy calibration was achieved by measuring a copper foil for the Cu edge and assigning the first inflection point of the Cu foil spectrum to 8980.3 eV. Data analysis was performed using the IFEFFIT package (*33*), including ATHENA for the data extraction and ARTEMIS for the shell fitting. E_0 was defined at the half-height of the absorption edge step. k^3-weighted EXAFS spectra were Fourier transformed over the k range of 3.7−12.8 Å^{-1} using a Kaiser-Bessel window (α = 2.0). Fits were performed on the Fourier filtered-spectra over the R range of 0.8−2.8 Å. Theoretical amplitude and phase shift functions were calculated with ab initio code FEFF version 7.0 (*34*) using structures for simple Cu−organic complexes from the Cambridge Structural Database (http://www.ccdc.cam.ac.uk/products/csd/).

Protease Digestion Experiments. Protease digestion experiments were conducted in a final volume of 50 μL containing CzcE at a concentration of 100 μM (dimer concentration). Cu(II)-bound forms of CzcE were produced by addition of 400 μM $CuCl_2$ dissolved extemporaneously in water. Cu(I)-bound

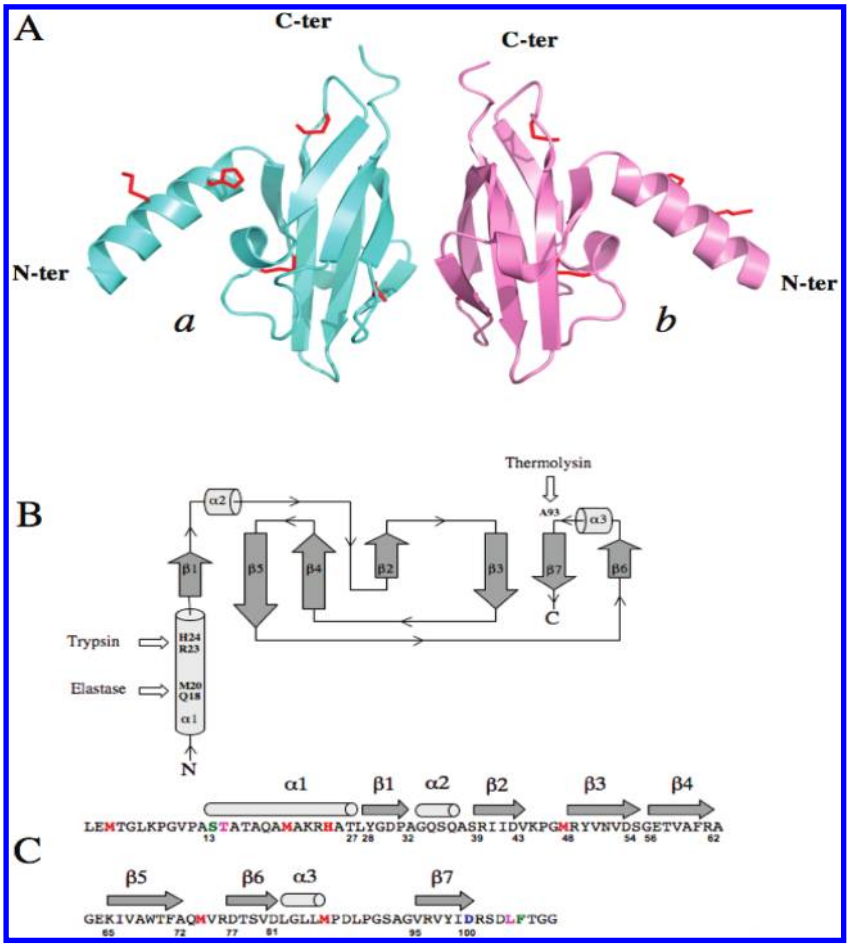

FIGURE 1: (A) Structure of the apo-CzcE dimer. Protomer *a* is colored cyan and protomer *b* pink. The side chains of some key residues potentially involved in Cu binding (His24 and the methionines except Met3 that did not appear in the electron density maps) are colored red. (B) Schematic representation of the CzcE protomer structural organization indicating the amino acids identified after proteolytic cleavage by the reported proteases. Note that α2 is a 3_{10}-helix and α3 is an α-helix. (C) CzcE sequence and distribution of the secondary structure elements. The initial and final residues for each helix and strand are indicated. His24 and the methionine residues are colored red. Asp100 is colored blue. The structurally defined N-terminal and C-terminal amino acids are colored green for protomer *a* (Ser13−Phe105) and magenta for protomer *b* (Thr14−Leu104). Structure figures have been generated with PyMOL (DeLano scientific LLC, San Carlos, CA).

CzcE was obtained anaerobically via addition of 1 mM sodium ascorbate to Cu(II)-bound CzcE in a glovebox under an overpressure of nitrogen. The different proteases were added at a 1/500 (w/w) enzyme/protein ratio, and proteolysis was allowed to proceed for 15 min at room temperature in the glovebox for Cu(I)-bound CzcE or in air for Cu(II)-bound CzcE. In each case, a control experiment without copper was run in parallel and under the same conditions. Reactions were stopped when the mixtures were heated in electrophoresis denaturing buffer, and the samples were immediately analyzed by SDS−PAGE (*35*).

RESULTS AND DISCUSSION

Structure of CzcE. As expected from preliminary diffraction data (*16*), the asymmetric unit of apo-czcE crystals contains two protomers, labeled *a* and *b*. They are linked by a noncrystallographic 2-fold symmetry. The model shown in Figure 1A encompasses residues 13−105 for protomer *a* and 14−104 for protomer *b* for a total of 108 residues in the sequence, N-terminal and C-terminal residues not being defined in the electron density map.

The core of each protomer consists of a sandwich of two β-sheets formed by seven polypeptide strands [β1−β7 (Figure 1B)] and including a 3_{10}-helix (residues 33−37, α2) and a short α-helix (residues 82−86, α3) that connect β1 to β2 and β6 to β7, respectively (Figure 1B,C). A N-terminal α-helix (α1) precedes β1 and protrudes from the β-core of each protomer. Strands β2 and β3 as well as the loop connecting them are involved in the contact region between the two protomers. The dimer stability is ensured by nine direct hydrogen bonds between residues. The dimer interface exhibits an important patch of acidic residues (Figure 2) contributed by four aspartate residues (Asp53, -77, -100, and -103) and one glutamate residue (Glu56) from each protomer. The X-ray structure of apo-CzcE does not exhibit any preformed metal-binding sites involving the histidine residues and the acidic residues (Asp and Glu) expected to provide nitrogen and oxygen ligands for the previously identified type 2 copper centers (*14*). On the other hand, the methionine residues, which can contribute to Cu(I) binding, are distributed in the sequence without structurally defining a metal-binding site. It should be noted that Met3 is not visible in this structure.

As crystals of the copper-bound form of CzeE had not yet been obtained, an extemporaneously prepared solution of $CuCl_2$ in water was added to crystals of apo-CzcE. In this way, three Cu atoms were localized using anomalous difference Fourier maps based on data collected at the Cu K absorption edge with phases calculated from the structure of the apoprotein. The root-mean-square deviation (rmsd) between the molecular structures of

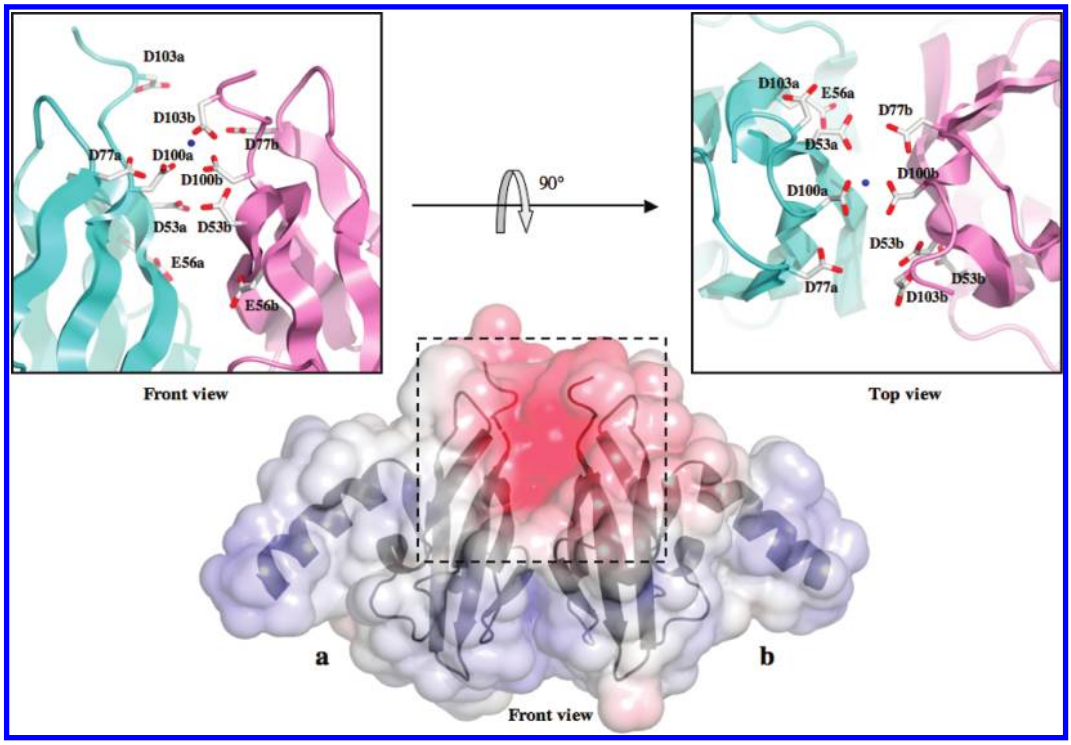

FIGURE 2: Charge distribution surface of the CzcE dimer (bottom). The red and blue areas represent negatively and positively charged surfaces, respectively. The acidic patch defining a negatively charged funnel is highlighted by a dotted-line square. The top left panel is a close-up view of this area in the same orientation. The side chains of the acidic amino acids present in the funnel are shown as sticks. These amino acids are identified by their one-letter code, their numbering in the sequence, and a lowercase letter corresponding to their protomer. The top right panel corresponds to a top view of the same area after a 90° rotation. The copper ion is depicted as a blue sphere. Note that only the side chains of both D100a and D100b face each other in both orientations.

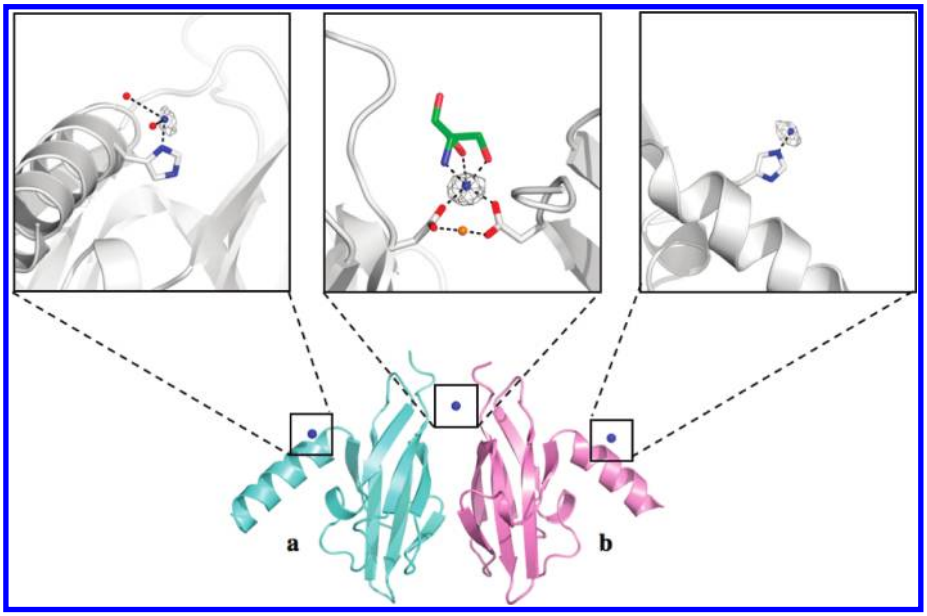

FIGURE 3: Three copper-binding sites identified after $CuCl_2$ soaking of the apo-CzcE crystals (bottom). Cu(II) ions are represented as blue spheres. The two water molecules identified in the coordination of copper in protomer *a* are colored red. The overall location of each site is framed and magnified in the top panels. Anomalous difference Fourier maps are contoured at 4σ, 6σ, and 10σ for sites in protomer *a*, in protomer *b*, and at the dimer interface, respectively. The close-up view of the dimer interface site shows that Asp100 is a bridging ligand for Cu(II) and Mg^{2+} (orange sphere). The coordination sphere of Cu(II) is completed by one N atom and one O atom in the equatorial plane coming from a Tris molecule (green sticks). The coordination sphere of Mg^{2+} is completed by three water molecules (not shown). Both Mg and Tris come from the crystallization conditions.

apo-CzcE and Cu-soaked CzcE calculated with 182 aligned Cα atoms pairs was 0.19 Å, indicating that no major structural changes occurred during metalation in the crystalline state. As expected, in each protomer one copper ion was located at the vicinity of His24 (Figure 3). In protomer *a*, the nitrogen ligand was provided by the imidazole Nδ1 atom that was 2.18 Å from the copper ion and in protomer *b* by the imidazole Nε2 atom that was 1.80 Å from the copper ion. Two oxygen atoms from water molecules were in the coordination sphere of the His-bound copper in protomer *a*. No other ligand either from the protein or

from the solvent was identified for His-bound copper in protomer *b*. A third Cu ion was located in the electronegative patch at the interface of the dimer (Figures 2 and 3). This Cu ion was tetracoordinated by two oxygen atoms from Asp100 carboxylates of protomers *a* and *b*, 2.09 and 1.90 Å from the Cu ion, respectively, and by one oxygen and one nitrogen from a Tris molecule trapped from the crystallization conditions. The number of copper ions and their respective coordination states deduced from Cu-soaked crystals reflect only partially what was expected for Cu-bound CzcE in solution (*14*). Conformational changes in the crystallized protein that allow the accommodation of four copper atoms in the structure are limited. For instance, helix α1, in which His24 is located, is involved in crystal packing contacts (not shown) and is thus immobilized. Asp100 is one of the five acidic residues per protomer that define a negatively charged patch at the interface of the dimer. This part of the protein forms a funnel that can attract cations toward its center. Indeed, a magnesium ion, trapped from the crystallization medium, was found in this funnel, close to the Cu ion with Asp100 from each protomer as a bridging ligand (Figure 3). Three water molecules completed the coordination sphere (not shown). This funnel could accommodate the forth Cu-binding site that remains to be identified.

The structure of apo-CzcE demonstrates that no metal-binding sites able to bind Cu(II) or Cu(I) are preformed in the protein and thus argues in favor of metal-dependent conformational changes. Because of the insertion of Tris and Mg^{2+}, and of the restricted possibilities of conformational changes, the metalled form obtained by soaking apoprotein crystals in a $CuCl_2$ solution is not relevant for the Cu-bound form in Hepes solution, i.e., the buffer used during purification. Nevertheless, it could correspond to an initial step of copper recognition before conformational changes leading to a definitive Cu-bound form. For instance, when ligands from the protein only (His24 and Asp100) are taken into account, the average distance between N or O and Cu is 1.99 Å, which is very close to the value of 1.97 ± 0.01 Å deduced from XAS experiments with Cu(II)-bound CzcE in solution (see below). In any case, the structure confirms that His24 is a Cu ligand in each protomer. It also revealed the participation of Asp100 from each protomer with a metal-binding site located on the interface of the dimer. His24 and Asp100 are key residues for copper binding, which was confirmed by a combination of site-directed mutagenesis and copper titration.

Spectrophotometric Changes in both Wild-Type and Mutated CzcE upon Cu Binding. Spectral changes were analyzed between 400 and 900 nm as a function of increasing amounts of $CuCl_2$ added to wild-type CzcE (wt-CzcE), H24A-CzcE, or D100N-CzcE (Figure 4). The titration of wt-CzcE by stepwise addition of 5 equiv of Cu(II) was characterized by a large featureless absorption band that increased almost linearly up to 4 equiv of Cu(II), the last spectrum indicating a saturation of the reaction. The two first bands had an absorbance maximum at 540 nm, while the following two exhibited a bathochromic shift at 550 nm and then 560 nm (Figure 4A). An average molar extinction coefficient of 66 M^{-1} cm^{-1} can be deduced from this experiment. The difference in absorption maximum suggests that the first two Cu ions are bound in a similar environment while those of the third and fourth Cu atoms are slightly different. These hypotheses are corroborated by the analysis of the titrations of H24A- and D100N-CzcE. For H24A-CzcE, the saturation was obtained for 2 equiv of Cu and the absorption bands were both centered at 540 nm (Figure 4B). This suggests the disappearance of two His24-dependent Cu-binding sites per CzcE dimer. The electronic absorption centered at 540 nm could thus be due to the other sites, including the site containing Asp100. Interestingly, 3 equiv of Cu was required to saturate D100N-CzcE, and three consecutive additions of 1 equiv of Cu led to the appearance of three consecutive bands centered at 540, 550, and 560 nm. This is in agreement with the disappearance of one copper-binding site located at the interface of the dimer and involving Asp100 in each protomer as shown by the structure determined from Cu-soaked crystals (Figures 2 and 3). On the other hand, only the first band was centered at 540 nm, while the next two displayed the bathochromic shifts that could be characteristic of the binding to His24. Under these conditions, the fourth site that remains to be identified in the wild-type protein must necessarily be located at the interface of the dimer and the anionic patch contributed by four Asp residues and one Glu residue from each protomer could accommodate the missing copper equivalent.

It must be noted that wt-CzcE was titrated with 4 equiv of Cu even in the presence of 200 mM $MgCl_2$ (data not shown), i.e., the $MgCl_2$ concentration used during crystallization. This strongly suggests that the Mg atom found in the structure did not take the place of a Cu atom. One can also speculate that the Cu-binding sites located in the acidic patch and giving the band at 540 nm have the highest affinity as they are filled before the sites involving His24. The two bathochromic shifts could be related to the imidazole nitrogen ligand that is different regardless of whether His24 belongs to protomer *a* or protomer *b* (Figure 3).

In separate experiments, the Cu(II)-bound form of each protein was produced via addition of the required amount of $CuCl_2$. Then, the protein was reduced by addition of a slight excess of ascorbate and allowed to reoxidize in air. The initial absorbance of the fully oxidized form was not reached after reoxidation, suggesting that H24A-CzcE and D100N-CzcE are also able to stabilize an air-stable semireduced state, as previously demonstrated with wt-CzcE (*14*). The absorbance maxima of semireduced H24A-CzcE remained centered at 540 nm (Figure 4E), while that of semireduced wt-CzcE or semireduced D100N-CzcE displayed a bathochromic shift of ~80 nm (panel D or F of Figure 4, respectively). This spectrum of semireduced wt-CzcE displayed a shoulder at 540 nm that was no longer visible for D100N-CzcE. This suggests that Asp100 remained a ligand in the semireduced form of both H24A-CzcE and wt-CzcE and participated in their spectra with a peak and a shoulder at 540 nm, respectively.

Metal Site Structure Explored by XAS. X-ray absorption spectroscopy (XAS) is the method of choice for structurally characterizing the copper-binding sites in the different oxidation states visited by the protein. This is particularly true for Cu(I)-bound CzcE that is EPR and UV−visible silent. Before XAS experiments, the specificity of the copper-binding sites was checked by assaying the amount of bound copper before and after filtration on a MicroBiospin-6 column. Copper ions bound strongly enough to the protein to remain present in both speciation states after being washed in the filtration column with metal-free buffer (not shown). Figure 5 shows the XAS data for CzcE in its fully oxidized and fully reduced state. The X-ray absorption near-edge structure (XANES) spectra show clear differences in the energy position and shape of the edge (Figure 5A). The broad edge in the spectrum for oxidized CzcE is typical of Cu(II) complexes, whereas the pre-edge at 8984 eV in the spectrum for reduced CzcE is characteristic of Cu(I)

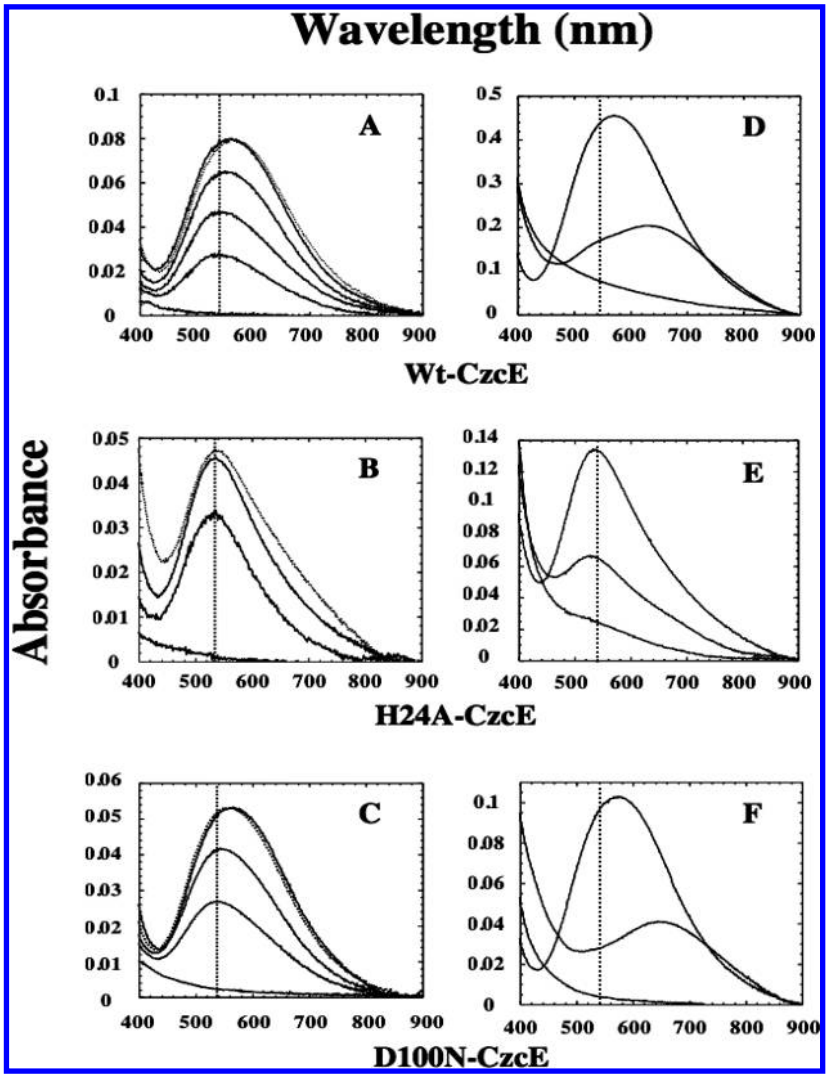

FIGURE 4: Visible spectroscopic characterization of wt-, H24A-, and D100N-CzcE. (A−C) Titration of 0.25 mM wt-CzcE (A), H24A-CzcE (B), and D100N-CzcE (C) in Hepes buffer with iterative addition of 1 equiv of $CuCl_2$. The dotted-line spectrum indicates the saturation of the reaction that was reached with 4 equiv of Cu for wt-CzcE, 2 equiv of Cu for H24A-CzcE, and 3 equiv of Cu for D100N-CzcE. The vertical line marks the wavelength of 540 nm that corresponds to the center of the electronic absorption after the addition of the first equivalent of Cu. Panels D−F display results of separate experiments in which 1.35 mM wt-CzcE (D), 0.8 mM H24A-CzcE (E), or 0.4 mM D100N-CzcE (F) was loaded with 4, 2, or 3 equiv of Cu, respectively (spectra with the highest intensity). Then, 2 equiv of ascorbate with respect to the initial copper concentration was added to produce the fully reduced form of the corresponding protein (spectra with the lowest intensity). Fully reduced proteins were allowed to reoxidize in air until the semireduced form stabilized (spectra with intermediate intensity).

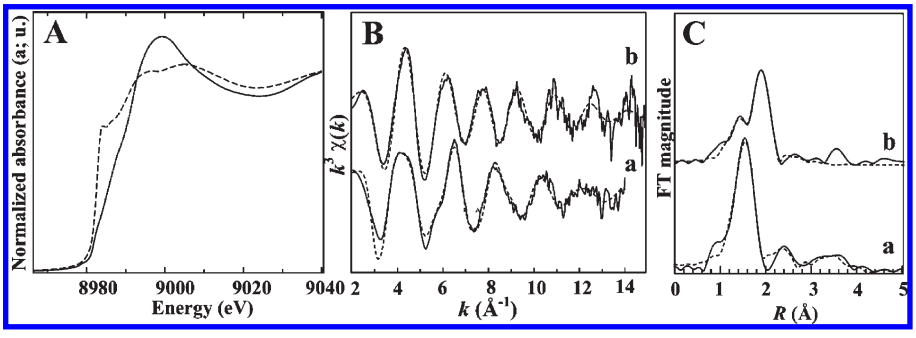

FIGURE 5: (A) Cu K edge XANES spectra for CzcE in reduced (---) and oxidized (—) states. (B−D) k^3-weighted EXAFS spectra (B) and Fourier transforms (non-phase-shift-corrected, C) for CzcE in the oxidized (a) or reduced (b) state: (—) experimental and (···) fits.

complexes (*36*, *37*). The Fourier transform spectrum for CzcE in the oxidized state presents an intense first peak typical of a first shell composed of O and N atoms (Figure 5C). Several characteristics (the relatively broad oscillation at 4 Å^{-1}, the shoulder at 6 Å^{-1} on the next oscillation, and the presence of second and third peaks at ~2.4 and ~3.5 Å, respectively, on the Fourier transform) suggest a weak multiple scattering effect typical of His ligands (*38*). Correct fits were obtained with a combination of N and O atoms at an average distance of 1.97 ± 0.01 Å, with the following constraints: $N_N \geq 1$, and $N_N + N_O = 4$ (Table 2). A mixed O/N shell is consistent with the X-ray data showing that His and Asp are ligands for Cu(II). The second shell was

fitted with 1.7 ± 0.6 C atoms at 2.88 ± 0.03 Å, and no multiple scattering effect was observed; the third shell was fitted with 1.9 ± 0.9 C or N atoms at 4.12 ± 0.03 Å and included multiple scattering contributions in the imidazole ring. This mixed O/N shell and the weak multiple scattering effect are consistent with the X-ray data showing that His and Asp are ligands for Cu(II). This is not surprising since in the hypothesis in which all copper atoms are 4-fold coordinated and one copper per monomer is bound to one His, the nitrogen from the imidazole ring would represent only one-eighth of the ligands. Still, supposing that His would account for one-eighth of the ligands for Cu(II), which corresponds to an N_N of 0.5 for Cu(II) in 4-fold coordination, other N ligands must be involved in Cu binding since $N_N \geq 1$. As the samples used for XAS experiments did not contain N ligands other than those proposed by the protein, we can imagine either nitrogen amide from the backbone or the N-terminus as a participant in the average Cu(II) coordination sphere as shown in other Cu-binding proteins (*39*, *40*).

The spectrum for CzcE in the reduced state presents a clearly higher frequency compared to that of oxidized CzcE (Figure 5B), and the first peak of the Fourier transform is split into two subpeaks (Figure 5C). The first one is centered at a slightly lower *R* value (atomic distance) compared to that of oxidized CzcE, and the second one is at a distance typical of S ligands. The first peak was fitted with a mixture of 1.2 ± 0.2 O or N atoms at 1.91 ± 0.02 Å and 1.8 ± 0.3 S atoms at 2.29 Å. No reliable fit was obtained with a total coordination number of 4. The second shell was composed of 1.4 ± 0.6 C atoms at 3.27 ± 0.05 Å. Because CzcE does not contain any cysteine, the sulfur-containing species coordinating Cu(I) atoms likely originate from the methionine residues. The Cu−S bond length of 2.29 Å is consistent with weak donors such as thioether ligands (*37*). As these structural parameters represent an average environment over the four Cu atoms present in the protein, we cannot certify that all Cu atoms occupy sites with mixed O/N and S ligands rather than sites containing S ligands only along with other ones containing O/N ligands. Pure O/N ligands for Cu(I) are very unlikely because Cu(I) is considered a soft metal and will preferably bind soft ligands such as sulfur atoms (*41*). Regardless, even if we are not able to discriminate between 2 or 3 S ligands, a Cu−S distance of 2.29 Å cannot be obtained without a conformational modification of the protein as judged from the positions of the methionine residues in apo-CzcE (Figure 1). For instance, the shortest distance between two S atoms in apo-CzcE is ~10 Å considering Met47 and Met86.

Table 2: Fits Obtained for the EXAFS of Fully Oxidized and Fully Reduced CzcE[a]

	atom	*N*	*R* (Å)	σ^2 (Å^2)	*R* factor ($\times 10^2$)
oxidized CzcE	N/O	4.0 (5)	1.97 (1)	0.007 (1)	2.5
	C	1.7 (6)	2.88 (3)	0.006 (2)	
	C/N[b]	1.9 (9)	3.25 (5)	0.012 (8)	
reduced CzcE	N/O	1.2 (2)	1.91 (2)	0.0083 (1)	0.7
	S	1.8 (3)	2.29 (1)	0.0083[c]	
	C	1.4 (6)	3.27 (5)	0.0083[c]	

[a] *N* is the number of atoms, *R* the interatomic distance, σ^2 the Debye−Waller factor, and *R* factor the residual between fit and experiment. Uncertainties in the last digit are given in parentheses. [b] This shell includes multiple scattering contributions within the imidazole ring. [c] Set equal to σ^2 for the first shell.

Susceptibility of CzcE to Protease Digestion. To determine the effect of Cu(II) or Cu(I) binding on CzcE conformation, the susceptibility of the protein to proteolysis was assayed with elastase, thermolysin, and trypsin for the apo form and both the Cu(II)- and Cu(I)-bound forms. As a control, each experiment was conducted with apo-CzcE under anaerobiosis or in air.

The proteolytic patterns shown in Figure 6 are all different. The presence of 4 equiv of Cu [either Cu(II) or Cu(I)] led to full protection against thermolysin action but to intermediate protection from trypsin action. On the other hand, only Cu(I)-bound CzcE was protected from elastase digestion. The product of each digestion was examined by electrospray mass spectrometry to determine the masses of the different peptides. We used the Findpept tool from ExPASy (http://www.expasy.org/tools/findpept.html) to identify the cleavage sites that are reported in Figure 1. Elastase and trypsin have both their cleavage sites in the first α-helix, while thermolysin cleaves CzcE at the C-terminus. Two fragments of 9602.89 and 9802.13 Da corresponding to Met20 and Gln18 as starting amino acids, respectively, were identified after elastase cleavage. Trypsin cleavage also led to two fragments of 9116.36 and 9272.43 Da corresponding to Arg23 and His24 as starting amino acids, respectively. The main fragment obtained by cleavage with thermolysin had a mass of 9602.83 Da and corresponded to a protein with Ala93 as C-terminal amino acid.

The copper speciation-dependent selectivity observed in the proteolysis pattern is also in agreement with conformational

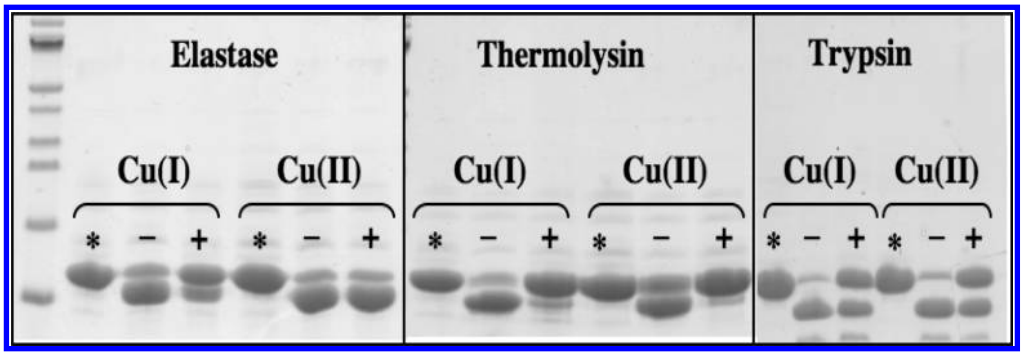

FIGURE 6: SDS−PAGE analysis of the CzcE proteolytic digests. Proteolysis was conducted for 15 min at room temperature as described in Materials and Methods. Protein was incubated with the indicated proteases [1/500 (w/w) enzyme/protein] in the absence of metal (−) or in the presence of 4 equiv of Cu (+). Cu(I)-bound CzcE was produced by reduction of Cu(II)-loaded CzcE with 10 equiv of ascorbate. Addition of ascorbate and incubation in the presence of the proteases were conducted in a glovebox under an overpressure of nitrogen to avoid reoxidation of the protein during the proteolysis process. A control in the absence of protease (asterisks) was run in parallel. The proteolytic fragments were identified by mass spectrometry.

changes upon metalation. Both elastase and trypsin action occurred on residues belonging to helix α1. Cu-dependent protection from trypsin cleavage and Cu(I)-specific protection from elastase cleavage are in agreement with the involvement of His24 and Met20 as key residues in Cu binding. One can speculate that upon binding of Cu(II) or Cu(I) to these amino acids, helix α1 initiates a movement toward the two-β-sheet core domain to complete the coordination sphere with other amino acids. One consequence of this movement could be the protection of the loop connecting helix α3 and strand β7 from thermolysin action.

CONCLUSION

In a previous study (*14*), we have suggested that CzcE could exist in vitro under three speciation states: fully oxidized containing 4 equiv of Cu(II), fully reduced containing 4 equiv of Cu(I), and an air stable semireduced form containing both 2 equiv of Cu(II) and 2 equiv of Cu(I). A rearrangement of the polypeptide chain was suspected to provide the appropriate ligands for Cu(I) and to explain the spectroscopic differences observed for Cu(II) in the fully oxidized form and the semireduced one. Our results show not only that conformational changes must occur for CzcE to accommodate 4 Cu(II) ions but also that a conformational modification of Cu local structure must occur between the two oxidation states, with Cu(II) bound to N and O ligands arranged in an average 4-fold coordination in the oxidized state, and Cu(I) bound to O/N and S ligands in an average 3-fold coordination in the reduced state.

CzcE is a new example of a protein able to accommodate copper under two speciation states. Under this criterion, it resembles CopC and PcoC, two copper-binding proteins belonging to copper resistance operons found in *E. coli* (*42*) and *Pseudomonas syringae* (*43*), respectively. In these latter proteins, two separated but interdependent binding sites specific for Cu(I) and Cu(II) were described as [Cu(I)(His)$(Met)_{2,3}$] and [Cu(II)-$(His)_2$(N-term)(OH_2)], respectively (*44*). The versatility of CzcE for Cu binding could be related to its genetic origin and its role in *C. metallidurans* CH34. CzcE is encoded by the *czc* cobalt−zinc−cadmium determinant (*10*) that arose from duplication of a core determinant composed of the *czcICAB* genes and from horizontal acquisition of other genes such as *czcN*, *czcD*, *czcRS*, and *czcE* (*9*). However, *czcE* itself is the product of the duplication of *copH* before being part of the *czc* determinant (*9*). As *czcE* and *copH* are thus strain-specific paralogs and as *copH* is involved in copper resistance (*1*−*6*) and encodes a copper-binding protein (*15*), it is not surprising that CzcE is also a copper-binding protein. CzcE might be a sentry in the periplasm acting as a Cu(I) and Cu(II) sensor and an actor of the multiple cross-responses of *C. metallidurans* CH34 against heavy metals by linking copper and cobalt−zinc−cadmium resistance.

ACKNOWLEDGMENT

We thank Guillaume Pompidor for his participation in X-ray data recording, Izabel Bérard for mass determination of Se-CzcE and of the CzcE mutants by mass spectrometry, Jean-Pierre Andrieu for the determination of the CzcE molar absorption coefficient, Isabelle Alliot, Florian Molton, Eric Lahera, and Olivier Proux for their help during XAS experiments, data recording, and processing, Yves Joly for XAS data modeling, and Antoine Maillard for critically reading the manuscript.

REFERENCES

1. Mergeay, M., Monchy, S., Vallaeys, T., Auquier, V., Benotmane, A., Bertin, P., Taghavi, S., Dunn, J., van der Lelie, D., and Wattiez, R. (2003) *Ralstonia metallidurans*, a bacterium specifically adapted to toxic metals: Towards a catalogue of metal-responsive genes. *FEMS Microbiol. Rev. 27*, 385–410.
2. Nies, D. H. (2003) Efflux-mediated heavy metal resistance in prokaryotes. *FEMS Microbiol. Rev. 27*, 313–339.
3. Noel-Georis, I., Vallaeys, T., Chauvaux, R., Monchy, S., Falmagne, P., Mergeay, M., and Wattiez, R. (2004) Global analysis of the *Ralstonia metallidurans* proteome: Prelude for the large-scale study of heavy metal response. *Proteomics 4*, 151–179.
4. Monchy, S., Benotmane, A., Wattiez, R., van Aelst, S., Auquier, V., Borremans, B., Mergeay, M., Taghavi, S., van der Lelie, D., and Vallaeys, T. (2006) Transcriptomic and proteomic analyses of the pMol30 encoded copper resistance in *Cupriavidus metallidurans* strain CH34. *Microbiology 152*, 1765–1776.
5. Monchy, S., Benotmane, M. A., Janssen, P., Vallaeys, T., Taghavi, S., van der Lelie, D., and Mergeay, M. (2007) Plasmids pMOL28 and pMOL30 of *Cupriavidus metallidurans* are specialized in the maximal viable response to heavy metals. *J. Bacteriol. 189*, 7417–7425.
6. Grosse, C., Friedrich, S., and Nies, D. H. (2007) Contribution of extracytoplasmic function sigma factors to transition metal homeostasis in *Cupriavidus metallidurans* strain CH34. *J. Mol. Microbiol. Biotechnol. 12*, 227–240.
7. Nies, D. H. (2000) Heavy metal-resistant bacteria as extremophiles: Molecular physiology and biotechnological use of *Ralstonia* sp. CH34. *Extremophiles 4*, 77–82.
8. Tibazarwa, C., Corbisier, P., Mench, M., Bossus, A., Solda, P., Mergeay, M., Wyns, L., and van der Lelie, D. (2001) A microbial biosensor to predict bioavailable nickel in soil and its transfer to plants. *Environ. Pollut.* (*Amsterdam, Neth.*) *113*, 19–26.
9. von Rozycki, T., and Nies, D. H. (2009) *Cupriavidus metallidurans*: Evolution of a metal-resistant bacterium. *Antonie van Leeuwenhoek 96*, 115–139.
10. Nies, D. H., Mergeay, M., Friedrich, B., and Schlegel, B. H. G. (1987) Cloning of plasmid genes encoding resistance to cadmium, zinc, and cobalt in *Alcaligenes eutrophus* CH34. *J. Bacteriol. 169*, 4865–4868.
11. van der Lelie, D., Schwuchow, T., Schwidetzky, U., Wuertz, S., Baeyens, W., Mergeay, M., and Nies, D. H. (1997) Two-component regulatory system involved in transcriptional control of heavy-metal homoeostasis in *Alcaligenes eutrophus*. *Mol. Microbiol. 23*, 493–503.
12. Grosse, C., Anton, A., Hoffmann, T., Franke, S., Schleuder, G., and Nies, D. H. (2004) Identification of a regulatory pathway that controls the heavy-metal resistance system Czc via promoter czcNp in *Ralstonia metallidurans*. *Arch. Microbiol. 182*, 109–118.
13. Legatski, A., Franke, S., Lucke, S., Hoffmann, T., Anton, A., Neumann, D., and Nies, D. H. (2003) First step towards a quantitative model describing Czc-mediated heavy metal resistance in *Ralstonia metallidurans*. *Biodegradation 14*, 153–168.
14. Zoropogui, A., Gambarelli, S., and Covès, J. (2008) CzcE from *Cupriavidus metallidurans* CH34 is a copper-binding protein. *Biochem. Biophys. Res. Commun. 365*, 735–739.
15. Sendra, V., Cannella, D., Bersch, B., Fieschi, F., Ménage, S., Lascoux, D., and Covès, J. (2006) CopH from *Cupriavidus metallidurans* CH34. A novel periplasmic copper-binding protein. *Biochemistry 45*, 5557–5566.
16. Pompidor, G., Zoropogui, A., Kahn, R., and Covès, J. (2007) Overproduction, purification and preliminary X-ray diffraction analysis of CzcE from *Cupriavidus metallidurans* CH34. *Acta Crystallogr. F63*, 884–886.
17. Van Duyne, G. D., Standaert, R. F., Karplus, P. A., Schreiber, S. L., and Clardy, J. (1993) Atomic structures of the human immunophilin FKBP-12 complexes with FK506 and rapamycin. *J. Mol. Biol. 229*, 105–124.
18. Pompidor, G., Girard, E., Maillard, A., Ramella-Pairin, S., Bersch, B., Kahn, R., and Covès, J. (2009) Biostructural analysis of the metal-sensor domain of CnrX from *Cupriavidus metallidurans* CH34. *Antonie van Leeuwenhoek 96*, 141–148.
19. Kabsch, W. (1988) Evaluation of single-crystal X-ray diffraction data from a position-sensitive detector. *J. Appl. Crystallogr. 21*, 916–924.
20. Collaborative Computational Project, Number 4 (1994) The CCP4 suite: Programs for protein crystallography. *Acta Crystallogr. D50*, 760–763.
21. Matthews, B. W. (1968) Solvent content of protein crystals. *J. Mol. Biol. 33*, 491–497.
22. Vonrhein, C., Blanc, E., Roversi, P., and Bricogne, G. (2007) Automated structure solution with autoSHARP. *Methods Mol. Biol. 364*, 215–230.

23. Schneider, T. R., and Scheldrick, G. M. (2002) Substructure solution with SHELXD. *Acta Crystallogr. D58*, 1772–1779.
24. De La Fortelle, E., and Bricogne, G. (1997) Maximum-likelihood heavy-atom parameter refinement for multiple isomorphous replacement and multiwavelength anomalous diffraction. *Methods Enzymol. 276*, 43–48.
25. Abrahams, J. P., and Leslie, G. W. (1996) Methods used in structure determination of bovine mitochondrial F_1 ATPase. *Acta Crystallogr. D52*, 30–42.
26. Cowtan, K. D., and Main, P. (1996) Phase combination and cross validation in iterated density-modification calculations. *Acta Crystallogr. D52*, 760–763.
27. Lamzin, V., Perrakis, A., and Wilson, K. (2001) The ARP/WARP suite for automated construction and refinement of protein models. International Tables for Crystallography. In Volume F: Crystallography of biological macromolecules (Rossman, M. G., and Arnold, E., Eds.) pp 720, Kluwer Academic Publishers, Dordrecht, The Netherlands.
28. Terwilliger, T. C., Grosse-Kunstleve, R. W., Afonine, P. V., Moriarty, N. W., Zwart, P. H., Hung, L.-W., Read, R. J., and Adams, P. D. (2008) Iterative model building, structure refinement and density modification with the PHENIX AutoBuild wizard. *Acta Crystallogr. D64*, 61–69.
29. Emsley, P., and Cowtan, K. (2004) Coot: Model-building tools for molecular graphics. *Acta Crystallogr. D60*, 2126–2132.
30. Brünger, A. (1992) Free R value: A novel statistical quantity for assessing the accuracy of crystal structures. *Nature 355*, 472–475.
31. Painter, J., and Merritt, E. A. (2006) TLSMDweb server for the generation of multi-group TLS models. *J. Appl. Crystallogr. 39*, 109–111.
32. Proux, O., Nassif, V., Prat, A., Ulrich, O., Lahera, E., Biquard, X., Menthonnex, J.-J., and Hazemann, J.-L. (2006) Feedback system of a liquid-nitrogen-cooled double-crystal monochromator: Design and performances. *J. Synchrotron Radiat. 13*, 59–68.
33. Ravel, B., and Newville, M. (2005) ATHENA and ARTEMIS: Interactive graphical data analysis using IFEFFIT. *J. Synchrotron Radiat. 12*, 537–541.
34. Rehr, J. J., Mustre de Leon, J., Zabinsky, S. I., and Albers, R. C. (1991) Theoretical X-ray absorption fine structure standards. *J. Am. Chem. Soc. 113*, 5135–5145.
35. Laemmli, U. K. (1970) Cleavage of structural proteins during the assembly of the head of bacteriophage T4. *Nature 227*, 680–685.
36. Kau, L.-S., Spira-Solomon, D. J., Penner-Hahn, J. E., Hodgson, K. O., and Solomon, E. I. (1987) X-ray absorption edge determination of the oxidation state and coordination number of copper: Application to the type 3 site in *Rhus vernicifera* laccase and its reaction with oxygen. *J. Am. Chem. Soc. 109*, 6433–6442.
37. D'Angelo, P., Pacello, F., Mancini, G., Proux, O., Hazemann, J.-L., Desideri, A., and Battistoni, A. (2005) X-ray absorption investigation of a unique protein domain able to bind both copper(I) and copper(II) at adjacent sites of the N-terminus of *Haemophilus ducreyi* Cu,Zn superoxide dismutase. *Biochemistry 44*, 13144–13150.
38. Strange, R. W., Blackburn, N. J., Knowles, P. F., and Hasnain, S. S. (1987) X-ray absorption spectroscopy of metal-histidine coordination in metalloproteins. Exact simulation of the EXAFS of tetrabis-(imidazole)copper(II) nitrate and other copper-imidazole complexes by the use of a multiple-scattering treatment. *J. Am. Chem. Soc. 109*, 7157–7162.
39. Aronoff-Spencer, E., Burns, C. S., Avdievich, N. I., Gerfen, G. J., Peisach, J., Antholine, W. E., Bal, H. L., Cohen, F. E., Prusiner, S. B., and Millhauser, G. L. (2000) Identification of the Cu^{2+} binding sites in the N-terminal domain of the prion protein by EPR and CD spectroscopy. *Biochemistry 39*, 13760–13771.
40. Rasia, R. M., Bertoncini, C. W., Marsh, D., Hoyer, W., Cherny, D., Zweckstetter, M., Griesinger, C., Jovin, T. M., and Fernandez, C. O. (2005) Structural characterization of copper(II) binding to α-synuclein: Insights into the bioinorganic chemistry of Parkinson's disease. *Proc. Natl. Acad. Sci. U.S.A. 102*, 4294–4299.
41. Bertini, I., and Turano, P. (2007) Metal ions and Proteins: Binding, stability, and folding. In Biological Inorganic Chemistry: Structure and Reactivity (Bertini, I., Gray, H. B., Stiefel, E. I., and Valentine, S. J., Eds.) pp 31, University Science Books, Sausalito, CA.
42. Brown, N. L., Barrett, S. R., Camakaris, J., Lee, B. T., and Rouch, D. A. (1995) Molecular genetics and transport analysis of the copper-resistance determinant (pco) form *Escherichia coli* plasmid pRJ1004. *Mol. Microbiol. 17*, 1153–1166.
43. Cooksey, D. A. (1994) Molecular mechanisms of copper resistance and accumulation in bacteria. *FEMS Microbiol. Rev. 14*, 381–386.
44. Djoko, K. Y., Xiao, Z., Huffman, D. L., and Wedd, A. G. (2007) Conserved mechanism of copper binding and transfer. A comparison of the copper-resistance proteins PcoC from *Escherichia coli* and CopC from *Pseudomonas syringae*. *Inorg. Chem. 46*, 4560–4568.